Influence of grain size and surface condition on minority-carrier lifetime in undoped n-BaSi2 on Si(111)

Ryota Takabe, Kosuke O. Hara, Masakazu Baba, Weijie Du, Naoya Shimada, Kaoru Toko, Noritaka Usami, and Takashi Suemasu

Citation: Journal of Applied Physics **115**, 193510 (2014); doi: 10.1063/1.4878159
View online: http://dx.doi.org/10.1063/1.4878159
View Table of Contents: http://scitation.aip.org/content/aip/journal/jap/115/19?ver=pdfcov
Published by the AIP Publishing

Influence of grain size and surface condition on minority-carrier lifetime in undoped *n*-$BaSi_2$ on Si(111)

Ryota Takabe,[1] Kosuke O. Hara,[2] Masakazu Baba,[1] Weijie Du,[1] Naoya Shimada,[1] Kaoru Toko,[1] Noritaka Usami,[2,3] and Takashi Suemasu[1,3]
[1]*Institute of Applied Physics, University of Tsukuba, Tsukuba, Ibaraki 305-8573, Japan*
[2]*Graduate School of Engineering, Nagoya University, Nagoya 464-8603, Japan*
[3]*Japan Science and Technology Agency, CREST, Tokyo 102-0075, Japan*

(Received 27 February 2014; accepted 5 May 2014; published online 21 May 2014)

We have fabricated approximately 0.5-μm-thick undoped *n*-$BaSi_2$ epitaxial films with various average grain areas ranging from 2.6 to 23.3 μm^2 on Si(111) by molecular beam epitaxy, and investigated their minority-carrier lifetime properties by the microwave-detected photoconductivity decay method at room temperature. The measured excess-carrier decay curves were divided into three parts in terms of decay rate. We characterized the $BaSi_2$ films using the decay time of the second decay mode, τ_{SRH}, caused by Shockley-Read-Hall recombination without the carrier trapping effect, as a measure of the minority-carrier properties in the $BaSi_2$ films. The measured τ_{SRH} was grouped into two, independently of the average grain area of $BaSi_2$. $BaSi_2$ films with cloudy surfaces or capped intentionally with a 3 nm Ba or Si layer, showed large τ_{SRH} (*ca.* 8 μs), whereas those with mirror surfaces much smaller τ_{SRH} (*ca.* 0.4 μs). X-ray photoelectron spectroscopy measurements were performed to discuss the surface region of the $BaSi_2$ films.
 [http://dx.doi.org/10.1063/1.4878159]

I. INTRODUCTION

In recent years, photovoltaic solar cells have received much attention. Although approximately 90% of solar cells are Si-based because of its earth-abundance and developed technologies, thin-film solar cell materials, such as chalcopyrites and CdTe, have been gaining increased attention from the viewpoint of their high optical absorption and cost effective growth procedure.[1–6] Thin-film Si solar cells have also been studied extensively to achieve high efficiencies by utilizing an efficient light trapping system;[7–17] however, it is not easy to achieve high efficiencies as large as 20%. Exploring alternative materials for thin-film solar cell applications is also very important. Among such materials, we have focused much attention on barium disilicide ($BaSi_2$). $BaSi_2$ has a large absorption coefficient of $3 \times 10^4\,cm^{-1}$ at 1.5 eV.[18] Besides, the band gap was found to be approximately 1.3 eV,[18–21] and increase up to 1.4 eV by replacing half of the Ba atoms with isoelectric Sr atoms.[22–25] Regarding the carrier concentration of $BaSi_2$, undoped $BaSi_2$ shows *n*-type conductivity with electron concentrations of about $10^{16}\,cm^{-3}$.[20] High hole concentrations exceeding $1 \times 10^{20}\,cm^{-3}$ were achieved in B-doped *p*-type $BaSi_2$.[26] Thus, we aim to realize a $BaSi_2$ *pn* diode using the undoped *n*-$BaSi_2$ as an optical absorption layer, and form the diode on a SiO_2 substrate capped with (111)-oriented Si layers by Al-induced crystallization.[27,28] Since *a*-axis-oriented $BaSi_2$ can be grown epitaxially on a Si(111) surface,[29,30] it is important to examine the minority-carrier properties of undoped *n*-$BaSi_2$ on Si(111). *a*-Axis-oriented $BaSi_2$ epitaxial films on Si(111) have three epitaxial variants rotated by 120° with each other around the surface normal.[30] The grain size of these $BaSi_2$ variants can be expanded from about 0.2 to 5 μm by adjusting the growth conditions for template layers.[31] Grain boundaries (GBs) in a semiconductor film often behave as recombination centers,[32] and thus deteriorate electrical and optical properties of the film. According to our previous work, we found that the minority-carrier lifetime in post-annealed undoped *n*-$BaSi_2$ was about 14 μs by the microwave-detected photoconductivity decay (μ-PCD) method.[33] This value is large enough for thin-film solar cell applications. We also evaluated the potential variations at the GBs in undoped *n*-$BaSi_2$ epitaxial films by Kelvin probe force microscopy (KFM), and presented that the concave band structure at the GBs may reduce the carrier recombination at the GBs.[34] On the basis of these results, we think that the GBs in undoped *n*-$BaSi_2$ do not act as recombination centers for photogenerated minority carriers (holes). However, we do not have sufficient data about GBs in $BaSi_2$. In this paper, we attempted to clarify whether the GBs affect the minority-carrier lifetime in the $BaSi_2$ films. For this purpose, we grew approximately 0.5-μm-thick undoped *n*-$BaSi_2$ epitaxial films with various grain areas on Si(111), namely, various densities of GBs. We use the term GBs to denote the boundaries of the epitaxial variants in this article.

II. EXPERIMENTAL METHOD

An ion-pumped molecular beam epitaxy (MBE) system equipped with an electron-beam evaporation source for Si and a standard Knudsen cell for Ba was used in this investigation. The details of the growth procedure are described in Ref. 35. Briefly, a $BaSi_2$ template layer was first grown by reactive deposition epitaxy (RDE), that is, Ba deposition on a hot floating-zone *n*-Si(111) substrate ($\rho > 1000\,\Omega$·cm).[36] The template layer works as a kind of seed crystals for subsequent layers. Next, Ba and Si were co-deposited on the template layer at 580 °C by MBE to form approximately

TABLE I. Sample preparation: $BaSi_2$ layer thickness, surface condition, and $BaSi_2$ average grain area by EBSD are specified.

Sample	Thickness (nm)	Surface	Average grain area (μm^2)
A	570	Mirror	2.6
B	420	Cloudy	8.3
C	450	Mirror	5.8
D	490	Cloudy	21.1
E	510	Cloudy	20.0
F	500	Cloudy	23.3

0.5-μm-thick undoped *n*-$BaSi_2$ epitaxial films. We prepared 8 samples with different grain sizes by changing the growth temperature during RDE and the Ba deposition rate.[31] Samples A-F were prepared as summarized in Table I. $BaSi_2$ films capped *in situ* with a 3 nm Ba (sample G) or Si (sample H) were also prepared as shown in Table II. The crystalline quality of the films was characterized by reflection high-energy electron diffraction (RHEED), x-ray diffraction (XRD) with Cu Kα radiation. RHEED patterns were observed along the Si[11$\bar{2}$] azimuth. In the XRD measurements, Ge(220) single crystals were used to make x-rays monochromatic. Electron backscatter diffraction (EBSD) analyses were performed in order to analyze the grain size of $BaSi_2$. The minority-carrier lifetime was measured by μ-PCD method. Electron-hole pairs were generated by a 5 ns laser pulse with a wavelength of 349 nm and photoconductivity decay was measured by the reflectivity of microwave with the frequency of 26 GHz.[37] The excitation laser intensity was varied from 1.1×10^2 to 1.3×10^5 W/cm^2, corresponding to the area photon density in the range 9.8×10^{11} to 1.1×10^{15} cm^{-2}, assuming no reflection on the $BaSi_2$ surface. X-ray photoelectron spectroscopy (XPS) was performed to analyze the composition of the surfaces. Monochromatic Al Kα radiation (1486.6 eV) was used for x-ray radiation source. The probing depth was set to be about 3 nm.

III. RESULTS AND DISCUSSION

Figure 1 shows the 12×12-μm^2 EBSD orientation maps and distribution histograms of grain area fraction in samples A-F. Average grain areas calculated from the histograms are also presented. We see three colors represented by red, blue, and green in the EBSD orientation maps, indicating that three epitaxial variants of *a*-axis-oriented $BaSi_2$ exist on Si(111).[30,35] The average grain area of $BaSi_2$ ranged from about 2.6 to 23.3 μm^2, depending on the growth conditions. It seems reasonable to suppose that the density of $BaSi_2$ GBs decreases with increasing average grain area.

TABLE II. Sample preparation: $BaSi_2$ layer thickness, capping, surface condition, and $BaSi_2$ average grain area by EBSD are specified.

Sample	Thickness (nm)	Capping (nm)	Surface	Average grain area (μm^2)
G	450	Ba (3)	Mirror	3.8
H	450	Si (3)	Mirror	5.9

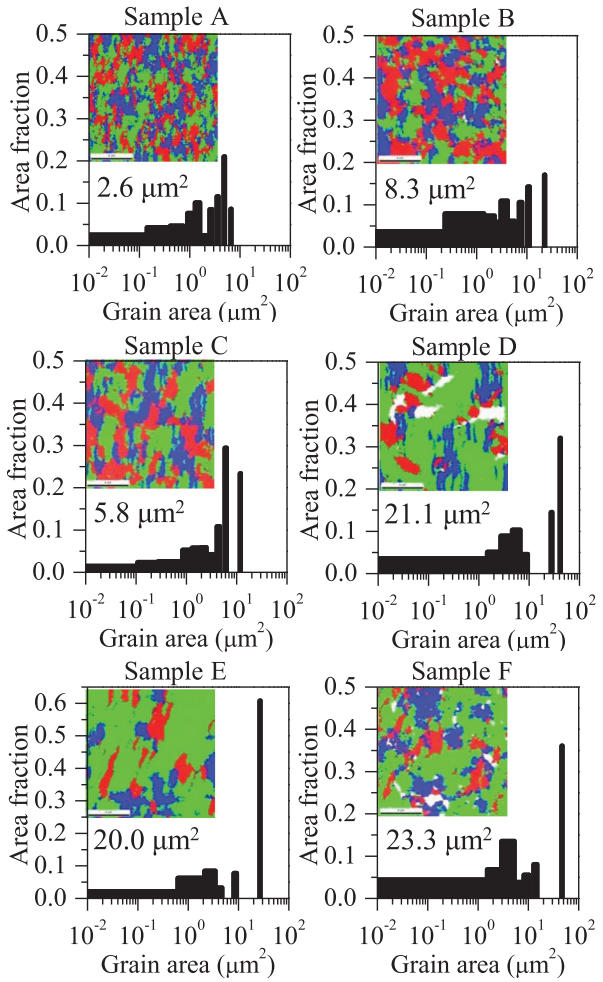

FIG. 1. 12×12-μm^2 EBSD crystal orientation maps of the $BaSi_2$ epitaxial films and distribution histograms of $BaSi_2$ grain area fraction in samples A-F. Average grain areas calculated from the histograms are also presented.

According to our previous work,[37] decay can be separated into three modes from the viewpoint of decay rate, and the decay curve was fitted well using Eq. (1)

$$I(t) = I_1 \exp\left(-\frac{t}{\tau_{\text{Auger}}}\right) + I_2 \exp\left(-\frac{t}{\tau_{\text{SRH}}}\right) + I_3 \exp\left(-\frac{t}{\tau_{\text{SRH-trapping}}}\right). \quad (1)$$

Here, I_1, I_2, and I_3 are the coefficients, and τ_{Auger}, τ_{SRH}, and $\tau_{\text{SRH-trapping}}$ the time constants for the three decay modes, that is, Auger recombination, and Shockley-Read-Hall (SRH) recombinations without and with the carrier trapping effect, respectively. Figure 2(a) shows the normalized μ-PCD decay curve of sample H. This is an example of typical decay curve. The inserted dotted lines correspond to the exponential decays of these three modes. Figures 2(b) and 2(c) shows the normalized μ-PCD decay curves of samples A and C, and samples B and D-F, respectively, when the excess carrier density, Δn, is 2.4×10^{18} cm^{-3}. Δn was calculated from the absorption coefficient of $BaSi_2$ at a wavelength of 349 nm, and irradiated laser intensity. $BaSi_2$ in

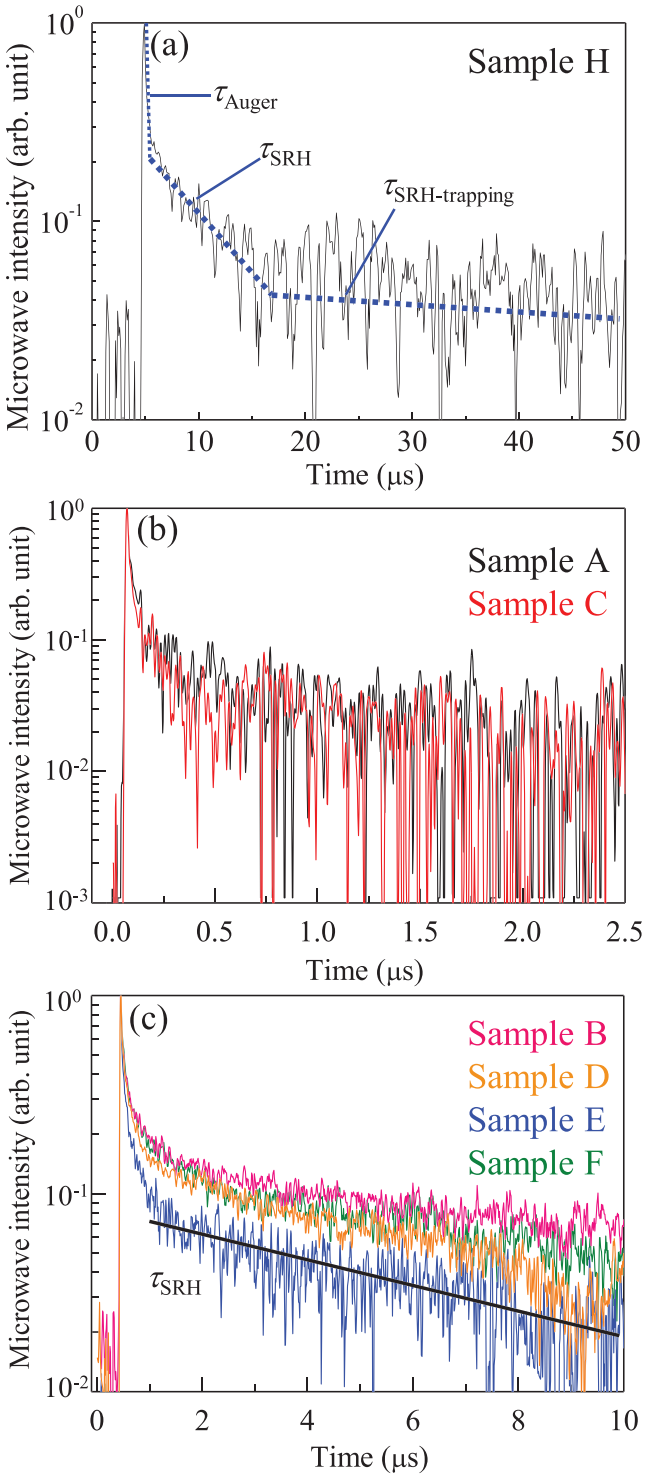

FIG. 2. (a) Normalized μ-PCD decay curves of (a) sample H, (b) samples A and C, and (c) samples B and D-F when Δn is 2.4×10^{18} cm^{-3}. The dotted lines in (a) correspond to the exponential decays with τ_{Auger}, τ_{SRH}, and $\tau_{SRH\text{-}trapping}$. The solid line in (c) shows the exponential decay with τ_{SRH} for sample E.

samples A and C showed much faster decay than the others as shown in Fig. 2(b). In Fig. 2(c), the decay curve in blue (sample E) was shifted downwards a little to be seen clearly. The inserted solid line shows the exponential decay with τ_{SRH}. In the SRH recombination, we assume a trap level in the band gap, where the recombination of electrons and holes occur via this level.[38] Since $BaSi_2$ is an indirect bandgap semiconductor, radiative recombination is less probable than the others. Slow decay with the carrier trapping effect corresponding to $\tau_{SRH\text{-}trapping}$ has been reported in silicon.[39–41] Of the three decay modes, the first and second decay modes denoted by τ_{Auger} and τ_{SRH}, respectively, are dominant. Basically what happens upon laser irradiation is that Auger recombination occurs in the initial stage because of a large absorption coefficient of $BaSi_2$ for the 349 nm light, and a high excitation in the μ-PCD measurement. The initial Δn at the surface reaches the range of 10^{18} to 10^{21} cm^{-3}. Thus, it is difficult to avoid the Auger recombination in the present μ-PCD measurement. Since there is an electric field in $BaSi_2$ due to the difference in electron affinity between $BaSi_2$ (3.2 eV)[42] and Si (4.0 eV), carrier separation occurs at the same time as Auger recombination, followed by the SRH recombination. In this work, we used τ_{SRH} as a measure to investigate the minority carrier properties of $BaSi_2$ films. This is because the first decay mode, Auger recombination, is not likely to happen in the actual AM 1.5 irradiation. Thus, the second decay mode is very important; τ_{SRH} should be larger enough to achieve high solar-cell efficiency. We measured the decay curves with changing irradiated laser intensity, and Δn was varied from 1.5×10^{16} to 2.4×10^{18} cm^{-3} on average. Figures 3(a) and 3(b) show examples of the dependences of τ_{SRH} on excess-carrier density measured on samples B and C, respectively. τ_{SRH} decreased with increasing Δn. This is because the Δn is orders of magnitude higher than the majority-carrier (electron) density, which is approximately 10^{16} cm^{-3}, at equilibrium in undoped n-$BaSi_2$. Such high carrier injection leads to multicarrier recombination. Therefore, we should use a low injection value when discussing the minority-carrier lifetime. As can be seen in Fig. 3, τ_{SRH} becomes almost independent of excess-carrier density when the Δn approaches 10^{16} cm^{-3}. This result makes sense because the electron concentration of undoped n-$BaSi_2$ is about 10^{16} cm^{-3}.[20] We, therefore, adopted the τ_{SRH} when Δn was about 10^{16} cm^{-3}.

Before we go into detailed discussions about τ_{SRH}, we need to mention a little about the difference between the bulk minority-carrier lifetime (14 μs) in our previous work[33] and τ_{SRH} in this work. The $BaSi_2$ layer thicknesses in samples A-H are around 0.5 μm. Thus, band bending is supposed to occur in the $BaSi_2$ films due to the difference in electron affinity between $BaSi_2$ and Si as described before. The

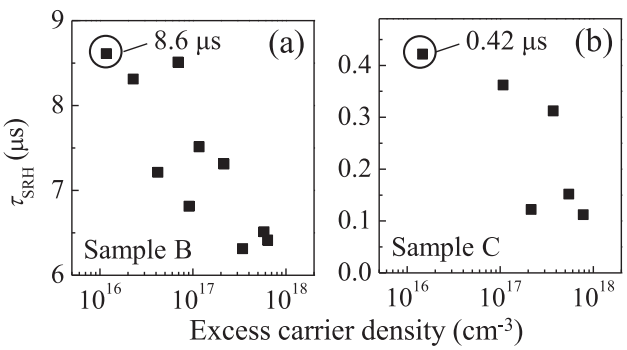

FIG. 3. Dependence of τ_{SRH} on excess-carrier density for (a) sample B and (b) sample C.

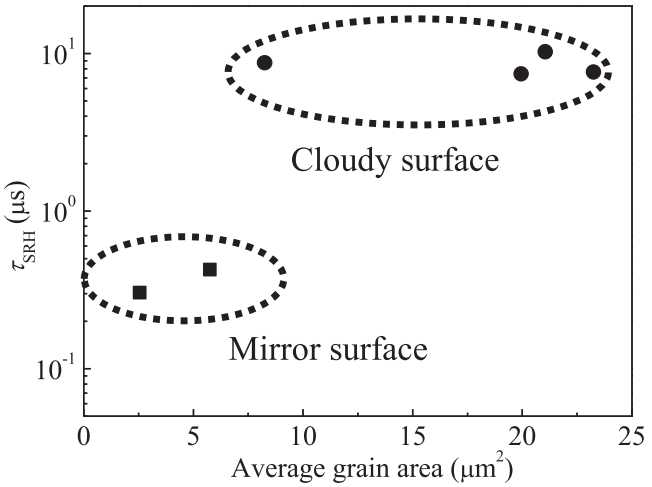

FIG. 4. Dependence of τ_{SRH} on $BaSi_2$ average grain area. The data points can be grouped into two denoted by dotted circles.

depletion width in $BaSi_2$ is estimated to be less than 0.4 μm. The photoexcited carriers are, therefore, expected to be separated in the $BaSi_2$, which makes τ_{SRH} larger. In contrast, the bulk minority-carrier lifetime of 14 μs was obtained for $BaSi_2$ films exceeding 1 μm in thickness. Thus, we cannot directly compare τ_{SRH} with this value (14 μs).

Figure 4 shows the dependence of τ_{SRH} on $BaSi_2$ average grain area. As can be seen in Fig. 4, τ_{SRH} values can be divided into two groups denoted by dotted circles, that is, approximately 0.4 and 8 μs. In each group, τ_{SRH} becomes almost the same, independently of $BaSi_2$ average grain area. This result implies that τ_{SRH} is not determined by GBs. This is consistent with what we expected from the potential variations around the GBs by KFM.[34] The important point here is that $BaSi_2$ with large τ_{SRH} had cloudy surfaces, whereas those with smaller τ_{SRH} mirror surfaces. In order to find out what caused this difference, we next investigated the crystalline quality of $BaSi_2$ in samples A-F.

Figure 5 shows the RHEED patterns of samples A and B taken just after the MBE growth of $BaSi_2$. Sharp streaky patterns are seen, and we do not see any distinct difference between them. Similar streaky RHEED patterns were observed for the other samples. For evaluation of the crystalline quality of the epitaxial films, full width at half maximum (FWHM) values obtained from an ω-scan x-ray rocking curve using a $BaSi_2$(600) diffraction peak were measured. We also evaluated the *a*-axis lattice constants of the $BaSi_2$ films from the XRD peak positions of $BaSi_2$(200), (400), and (600) diffractions. Figures 6(a) and 6(b) show the relationships between τ_{SRH} and FWHM of $BaSi_2$(600) peak intensity, and τ_{SRH} and *a*-axis lattice constant of $BaSi_2$, respectively. We see that τ_{SRH} neither depends on FWHM of $BaSi_2$(600) peak intensity nor on *a*-axis lattice constant, meaning that the crystallographic difference does not influence significantly on τ_{SRH}. We can thereby safely state that the difference in τ_{SRH} is attributed to sample surfaces. Actually, it was when the samples were exposed to air that their surfaces started to become cloudy in samples B and D-F. Since a large number of carriers are generated in the width of 50 nm from the surface with an ultraviolet excitation source (349 nm) in the μ-PCD measurements, τ_{SRH} is supposed to be sensitive to the $BaSi_2$ surfaces.

In order to clarify the surface composition and bonding states we performed XPS measurements. The XPS spectra of Ba $3d_{5/2}$, O 1*s*, Si 2*p*, and C 1*s* states for sample A (mirror surface) and sample B (cloudy surface) are shown in Figs. 7(a)–7(d), respectively. Similar results were obtained for samples C-F. The peak position of Ba $3d_{5/2}$ state for not oxidized $BaSi_2$ due to *in situ* CaF_2 capping was also shown in Fig. 7(a).[43] The broad peak around 532 eV in Fig. 7(b) originates from Ba-related oxides such as BaO and $BaCO_3$, and BaOH.[44–46] Hydrocarbons due to surface contaminations also exist. We attribute the broad peak around 103 eV to Si-related oxides such as SiO_2 and $SiO_x(x < 2)$, and that

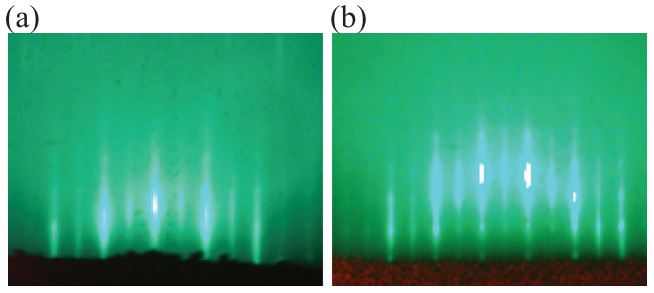

FIG. 5. RHEED patterns observed along the Si[11$\bar{2}$] azimuth for (a) sample A and (b) sample B just after the MBE growth of $BaSi_2$.

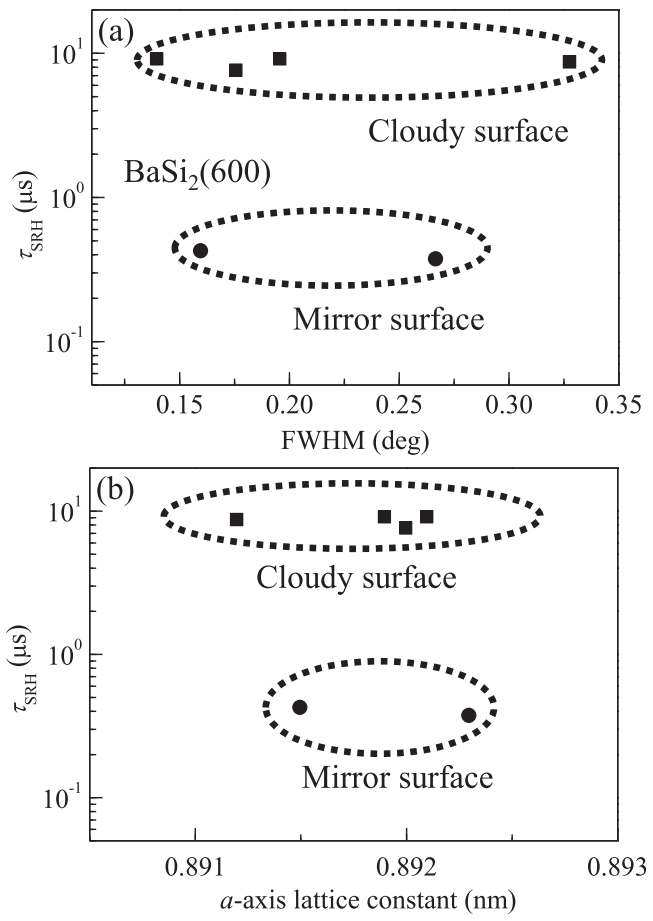

FIG. 6. Relationships between (a) τ_{SRH} and $BaSi_2$(600) FWHM, and (b) τ_{SRH} and *a*-axis lattice constant of $BaSi_2$.

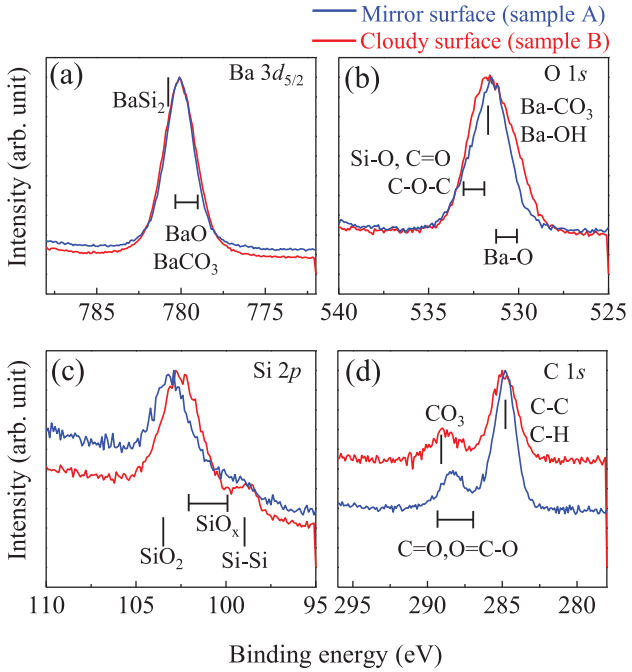

FIG. 7. Normalized XPS spectra of (a) Ba $3d_{5/2}$, (b) O 1*s*, (c) Si 2*p*, and (d) C 1*s* states for samples A (mirror surface) and B (cloudy surface). The peak position of not oxidized $BaSi_2$[43] is also shown in (a).

around 99 eV to Si.[47] However, we see no distinct difference in XPS spectra between samples A and B, in contrast to our prediction. Another problem with these $BaSi_2$ films in samples A-F was that we were not able to control the surface of $BaSi_2$ regarding whether it became cloudy or remained mirror after we exposed them to air. This means that the formation of $BaSi_2$ films with longer τ_{SRH} was out of control.

In order to control the $BaSi_2$ surface, we next grew two samples G and H, that is, 450 nm-thick $BaSi_2$ epitaxial films, followed by capping with a 3 nm Ba or Si layer at low temperatures (100 °C), respectively. These $BaSi_2$ films showed mirror surfaces. Figure 8 shows the 12×12-μm^2 EBSD orientation maps and distribution histograms of grain area fraction in samples G and H. Average grain areas calculated from the histograms are also presented, which were 3.8 and 5.9 μm^2, respectively. The important result is that the μ-PCD measurements revealed that τ_{SRH} was approximately 10 and 7 μs, respectively, as shown in Fig. 9. This means that the

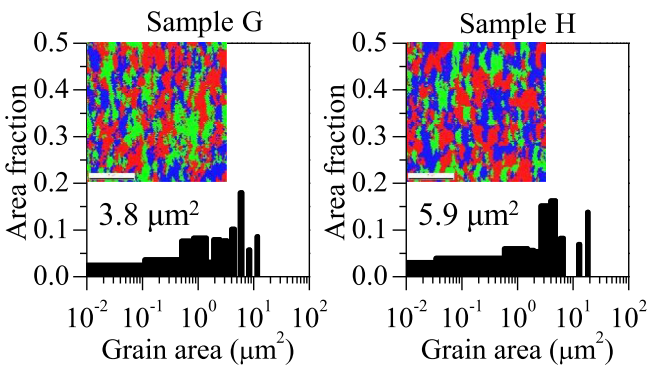

FIG. 8. 12×12-μm^2 EBSD crystal orientation maps of the $BaSi_2$ epitaxial films and distribution histograms of $BaSi_2$ grain area fraction in samples G and H. Average grain areas calculated from the histograms are also presented.

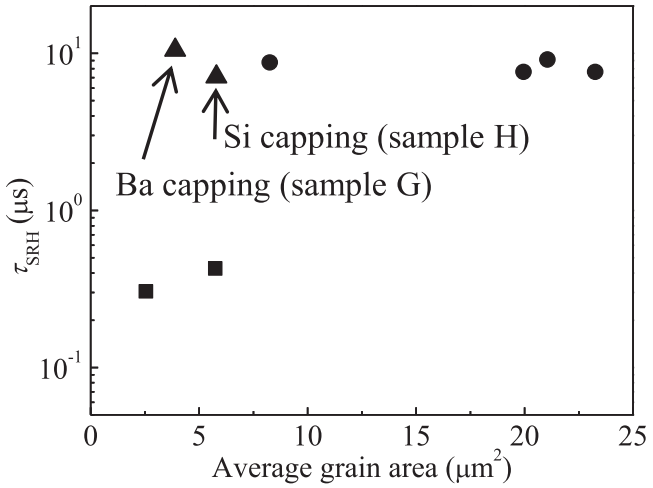

FIG. 9. Dependence of τ_{SRH} on average grain area of $BaSi_2$ for all the samples.

τ_{SRH} was almost the same as those with cloudy surfaces. This result is a significant progress because the capping with a Ba or Si layer enabled us to intentionally form $BaSi_2$ films with large τ_{SRH}. In order to investigate the surface of these $BaSi_2$ films, XPS measurements were also performed as shown in Fig. 10. The distinct peaks in the Ba $3d_{5/2}$, O 1*s*, and C 1*s* states suggest the existence of oxides such as $BaCO_3$ and BaO, and others like BaOH and hydrocarbons in sample G, $BaSi_2$ capped with the Ba layer. On the other hand, oxidation of Si was promoted in sample H, $BaSi_2$ capped with the Si layer. These results seem reasonable to suppose that the topmost Ba and Si layers got oxidized after the exposure of samples to air. However, it is difficult to identify the origin of large τ_{SRH} in samples B, G, and H from the XPS spectra shown in Figs. 7 and 10. Table III presents

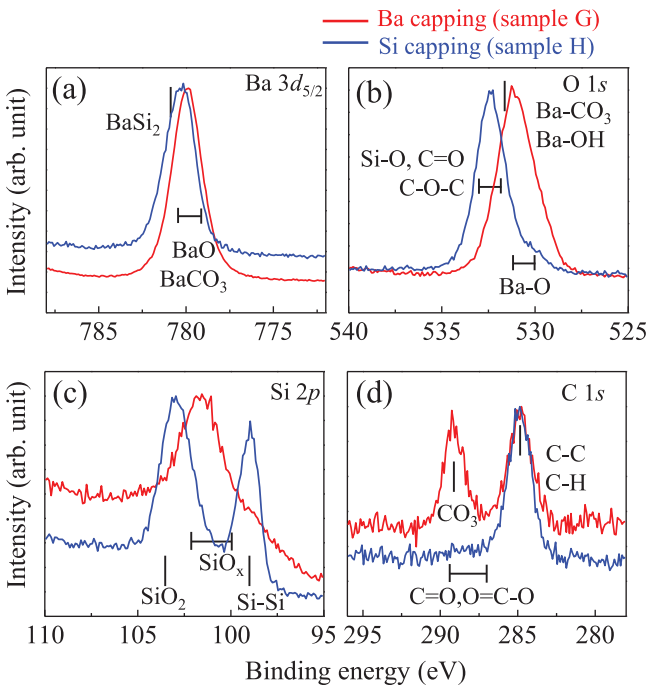

FIG. 10. Normalized XPS spectra of (a) Ba $3d_{5/2}$, (b) O 1*s*, (c) Si 2*p*, and (d) C 1*s* states for samples G (mirror surface) and H (mirror surface).

TABLE III. Relative elemental compositions of Ba, O, Si, and C in the surface regions of $BaSi_2$ in samples A, B, G, and H, measured by XPS.

Sample	Ba	O	Si	C
A	6.3	33.8	7.4	52.5
B	9.7	45.8	17.0	27.5
G	15.6	49.3	13.0	22.1
H	3.7	46.3	31.6	18.3

the relative elemental composition of Ba, O, Si, and C atoms in the surface region of $BaSi_2$ in samples A, B, G, and H. We see that the O ratio is smaller only in sample A than those in the other three samples. Considering the fact that τ_{SRH} was much smaller only in sample A among the above four samples, one explanation is that O atoms have something to do with large τ_{SRH}. Our previous finding of extremely low surface recombination velocity (8.3 cm/s)[33] of annealed $BaSi_2$ films may also be attributed to the existence of thin oxidized layer, which was formed by annealing. Surface passivation is widely known in Si capped with oxides such as SiO_2 and Al_2O_3.[48–53] At present, we do not have sufficient data to discuss with further. Thus, further studies are mandatory; however, we may reasonably conclude that it is not the GBs but the surface that significantly influence the τ_{SRH}, thereby minority-carrier lifetime in the $BaSi_2$ epitaxial films on Si(111). It is also safely stated that the capping with a Ba or Si layer enables us to form $BaSi_2$ films with large τ_{SRH}.

IV. SUMMARY

We fabricated approximately 0.5-μm-thick *a*-axis oriented undoped *n*-$BaSi_2$ epitaxial films with various average grain areas ranging from 2.6 to 23.3 μm^2 on Si(111) by MBE, and measured their τ_{SRH} as a measure of minority-carrier properties. $BaSi_2$ films with mirror surfaces showed small τ_{SRH} (*ca.* 0.4 μs), while those with cloudy surfaces much larger τ_{SRH} (*ca.* 8 μs). τ_{SRH} did not depend on the average grain area of $BaSi_2$, but significantly on the surface condition of these films. The problem was that we were not able to control the surface of $BaSi_2$ films to become either mirror or cloudy after exposed to air. This problem was solved by the *in situ* capping with a 3 nm Ba or Si layer on $BaSi_2$, enabling us to intentionally form $BaSi_2$ with large τ_{SRH}. The τ_{SRH} was as large as those in $BaSi_2$ films with cloudy surfaces. This is an important achievement for solar cell applications of $BaSi_2$. The XPS analyses implied that the O atoms may play an important role to make τ_{SRH} large.

ACKNOWLEDGMENTS

This work was supported in part by the Core Research for Evolutional Science and Technology (CREST) project of the Japan Science and Technology Agency (JST), and by Grants-in-Aid for Challenging Exploratory Research (No. 23655200) from the Ministry of Education, Culture, Sports, Science and Technology (MEXT) of Japan.

[1]A. Romeo, A. Terheggen, D. Abou-Ras, D. L. Batzner, F. J. Haug, M. Kalin, D. Rudmann, and A. N. Tiwari, Prog. Photovoltaics **12**, 93 (2004).
[2]I. Repins, M. A. Contreras, B. Egaas, C. DeHart, J. Scharf, C. L. Perkins, B. To, and R. Noufi, Prog. Photovoltaics **16**, 235 (2008).
[3]P. Jackson, D. Hariskos, E. Lotter, S. Paetel, R. Wuerz, R. Menner, W. Wischmann, and M. Powalla, Prog. Photovoltaics **19**, 894 (2011).
[4]H. Katagiri, K. Jimbo, W. S. Maw, K. Oishi, M. Yamazaki, H. Araki, and A. Takeuchi, Thin Solid Films **517**, 2455 (2009).
[5]J. Britt and C. Ferekides, Appl. Phys. Lett. **62**, 2851 (1993).
[6]X. Wu, Sol. Energy **77**, 803 (2004).
[7]R. G. Gordon, J. Proscia, F. B. Ellis, Jr., and A. E. Delahoy, Sol. Energy Mater. **18**, 263 (1989).
[8]P. Campbell, Sol. Energy Mater. **21**, 165 (1990).
[9]H. Sasaki, H. Morikawa, Y. Matsuno, M. Deguchi, T. Ishihara, H. Kumabe, T. Murotani, and S. Mitsui, Jpn. J. Appl. Phys., Part 1 **33**, 3389 (1994).
[10]J. Meier, S. Dubail, R. Platz, P. Torres, U. Kroll, J. A. A. Selvan, N. P. Vaucher, Ch. Hof, D. Fischer, H. Keppner, R. Flückiger, A. Shah, V. Shklover, and K.-D. Ufert, Sol. Energy Mater. Sol. Cells **49**, 35 (1997).
[11]O. Vetterl, F. Finger, R. Carius, P. Hapke, L. Houben, O. Kluth, A. Lambertz, A. Mück, B. Rech, and H. Wagner, Sol. Energy Mater. Sol. Cells **62**, 97 (2000).
[12]A. Poruba, A. Fejfar, Z. Remes, J. Springer, M. Vanecek, and J. Kocka, J. Appl. Phys. **88**, 148 (2000).
[13]J. Müller, B. Rech, J. Springer, and M. Vanecek, Sol. Energy **77**, 917 (2004).
[14]M. Berginski, J. Hüpkes, M. Schulte, G. Schöpe, H. Stiebig, and B. Rech, J. Appl. Phys. **101**, 074903 (2007).
[15]D. Zhou and R. Biswas, J. Appl. Phys. **103**, 093102 (2008).
[16]A. Hongsingthong, T. Krajangsang, I. A. Yunaz, S. Miyajima, and M. Konagai, Appl. Phys. Express **3**, 051102 (2010).
[17]H. Sai, Y. Kanamori, and M. Kondo, Appl. Phys. Lett. **98**, 113502 (2011).
[18]K. Toh, T. Saito, and T. Suemasu, Jpn. J. Appl. Phys., Part 1 **50**, 068001 (2011).
[19]T. Nakamura, T. Suemasu, K. Takakura, F. Hasegawa, A. Wakahara, and M. Imai, Appl. Phys. Lett. **81**, 1032 (2002).
[20]K. Morita, Y. Inomata, and T. Suemasu, Thin Solid Films **508**, 363 (2006).
[21]S. Kishino, T. Imai, T. Iida, Y. Nakaishi, M. Shinada, Y. Takanashi, and N. Hamada, J. Alloys Compd. **428**, 22 (2007).
[22]Y. Inomata, T. Suemasu, T. Izawa, and F. Hasegawa, Jpn. J. Appl. Phys., Part 2 **43**, L771 (2004).
[23]K. Morita, Y. Inomata, and T. Suemasu, Jpn. J. Appl. Phys., Part 2 **45**, L390 (2006).
[24]Y. Imai and A. Watanabe, Thin Solid Films **515**, 8219 (2007).
[25]M. Imai, A. Saito, T. Aoyagi, T. Kimura, and Y. Mori, Intermetallics **18**, 548 (2010).
[26]M. Ajmal Khan, K. O. Hara, W. Du, M. Baba, K. Nakamura, M. Suzuno, K. Toko, N. Usami, and T. Suemasu, Appl. Phys. Lett. **102**, 112107 (2013).
[27]O. Nast, T. Puzzer, L. M. Koschier, A. B. Sproul, and S. R. Wenham, Appl. Phys. Lett. **73**, 3214 (1998).
[28]R. Numata, K. Toko, N. Saitoh, N. Yoshizawa, N. Usami, and T. Suemasu, Cryst. Growth Des. **13**, 1767 (2013).
[29]R. A. Mackee, F. J. Walker, J. R. Conner, and R. Raj, Appl. Phys. Lett. **63**, 2818 (1993).
[30]Y. Inomata, T. Nakamura, T. Suemasu, and F. Hasegawa, Jpn. J. Appl. Phys., Part 2 **43**, L478 (2004).
[31]M. Baba, K. Nakamura, W. Du, M. A. Khan, S. Koike, K. Toko, N. Usami, N. Saito, N. Yoshizawa, and T. Suemasu, Jpn. J. Appl. Phys. **51**, 098003 (2012).
[32]I. Gordon, L. Carnel, D. Van Gestel, G. Beaucarne, and J. Poortmans, Thin Solid Films **516**, 6984 (2008).
[33]K. O. Hara, N. Usami, K. Nakamura, R. Takabe, M. Baba, K. Toko, and T. Suemasu, Appl. Phys. Express **6**, 112302 (2013).
[34]M. Baba, S. Tsurekawa, K. Watanabe, W. Du, K. Toko, K. O. Hara, N. Usami, T. Sekiguchi, and T. Suemasu, Appl. Phys. Lett. **103**, 142113 (2013).
[35]R. Takabe, K. Nakamura, M. Baba, W. Du, M. A. Khan, K. Toko, M. Sasase, K. O. Hara, N. Usami, and T. Suemasu, Jpn. J. Appl. Phys. **53**, 04ER04 (2014).
[36]Y. Inomata, T. Nakamura, T. Suemasu, and F. Hasegawa, Jpn. J. Appl. Phys., Part 1 **43**, 4155 (2004).
[37]K. O. Hara, N. Usami, K. Toh, M. Baba, K. Toko, and T. Suemasu, J. Appl. Phys. **112**, 083108 (2012).
[38]W. Shockley and W. T. Read, Jr., Phys. Rev. **87**, 835 (1952).
[39]J. A. Hornbeck and J. R. Haynes, Phys. Rev. **97**, 311 (1955).
[40]D. Macdonald and A. Cuevas, Appl. Phys. Lett. **74**, 1710 (1999).

[41]Y. Hu, H. Schøn, Ø. Nielsen, E. Johannes Øvrelid, and L. Arnberg, J. Appl. Phys. **111**, 053101 (2012).
[42]T. Suemasu, K. Morita, M. Kobayashi, M. Saida, and M. Sasaki, Jpn. J. Appl. Phys., Part 2 **45**, L519 (2006).
[43]M. Baba, K. Ito, W. Du, T. Sanai, K. Okamoto, K. Toko, S. Ueda, Y. Imai, A. Kimura, and T. Suemasu, J. Appl. Phys. **114**, 123702 (2013).
[44]J. A. T. Verhoeven and H. van Doveren, Appl. Surf. Sci. **5**, 361 (1980).
[45]T. L. Barr, J. Vac. Sci. Technol. A **9**, 1793 (1991).
[46]P. J. Schmitz, Surf. Sci. Spectra **8**, 190 (2001).
[47]F. J. Grunthaner, P. J. Grunthaner, R. P. Vasquez, B. F. Lewis, J. Maserjian, and A. Madhukar, J. Vac. Sci. Technol. **16**, 1443 (1979).
[48]A. W. Stephens, A. G. Aberle, and M. A. Green, J. Appl. Phys. **76**, 363 (1994).
[49]S. W. Glunz, A. B. Sproul, W. Warta, and W. Wettling, J. Appl. Phys. **75**, 1611 (1994).
[50]H. Kobayashi, A. Asano, S. Asada, T. Kubota, Y. Yamashita, K. Yoneda, and Y. Todoroki, J. Appl. Phys. **83**, 2098 (1998).
[51]A. G. Aberle, Prog. Photovoltaics **8**, 473 (2000).
[52]B. Hoex, S. B. S. Heil, E. Langereis, M. C. M. van de Sanden, and W. M. M. Kessels, Appl. Phys. Lett. **89**, 042112 (2006).
[53]J. Schmidt, A. Merkle, R. Brendel, B. Hoex, M. C. M. van de Sanden, and W. M. M. Kessels, Prog. Photovoltaics **16**, 461 (2008).